

**A Control Volume Finite
Element Method for Local Mesh
Refinement in Thermal Reservoir
Simulation**

by

P.A. Forsyth

Research Report CS-88-15
April, 1988

A Control Volume Finite Element Method for Local Mesh Refinement in Thermal Reservoir Simulation

P.A. Forsyth

Department of Computer Science
University of Waterloo
Waterloo, Ontario
N2L 3G1

ABSTRACT

This paper describes a control volume-finite element technique for coupling coarse grids with local fine meshes. The pressure is treated in a finite element manner, while the mobility terms are upstream weighted in the usual way. This requires identification of the cell volumes and edges which are consistent with the linear finite element discretization of the pressure. In order to ensure that the pressure equation yields an M -matrix, various conditions are required for the type of triangulation allowed. Since the form of the equations is similar to the usual finite difference discretization, standard techniques can be used to solve the Jacobian. The local mesh refinement method is demonstrated on some thermal reservoir simulation problems, and computational results presented. Significant savings in execution times are obtained while giving similar predictions to global fine mesh runs.

Introduction

Local and dynamic mesh refinement are useful methods for obtaining high resolution of shock fronts and near wellbore flow in reservoir simulation [1-6]. This is particularly important in modelling cyclic steam injection which is used to recover high viscosity crude oil [7-9].

Typically, control volume based finite difference methods are used to discretize the system of equations representing multi-phase heat and mass transfer in a porous medium [10,11]. These equations are highly non-linear, and of mixed hyperbolic-

parabolic type. Phase upstream weighting is used for mobility terms. In certain cases, phase upstream weighting can be shown to converge to the physically correct solution satisfying the entropy condition [12].

If the usual finite element method could be used, it would be a simple matter to generate a locally refined discretization. However, it is difficult to combine upstream weighting and the finite element method for multi-dimensional, multi-phase flows. It is possible to use an asymmetric weighting function [13], but this does not ensure that saturations will remain positive, in the absence of interphase mass transfer. This is especially important in thermal problems, where interphase mass transfer does take place. In this situation, the appearance of negative saturation values indicates violation of a thermodynamic constraint [8,11]. Consequently, since multi-phase flows with heat transfer are very complex, it is desirable to retain the easy physical interpretation of control volume methods, while at the same time obtaining some of the intrinsic flexibility of the finite element method.

Although the techniques used in this article are quite general, we will restrict attention to the problem of local mesh refinement in reservoir simulation. In particular, the problem of coupling the local fine mesh to the global coarse mesh will be considered. Two methods have been proposed for achieving this coupling. One technique uses a very low order coupling for the pressure [1,3]. In fact, the truncation error for this scheme is formally of $O(1/h)$, where h is a measure of the grid size. However, a more subtle analysis shows that this scheme is convergent, but the convergence can be slow in any region within $O\{h \log(1/h)\}$ of the interface [14]. This technique has the advantage that in the single phase limit, the pressure is given by the solution of an M -matrix, which ensures that no non-physical local maxima and minima can occur [15]. Although this method is often effective, some flow situations give inaccurate results [4]. An alternative is to use interpolation to obtain a high order coupling [4,16]. However, this reduces the diagonal dominance of the Jacobian, which can lead to difficulties for an iterative solver, unless some of the terms are evaluated explicitly. As well, in the single phase limit, the pressure matrix is not an M -matrix, which can have undesirable consequences.

The control volume finite element method has been proposed as a technique for Navier-Stokes flows [17,18], which allows flexible grids. This method is similar to the box method in semi-conductor device modelling [19,20]. Similar ideas were also proposed by Varga [15]. In the following, we will apply the control volume-finite element method to thermal reservoir simulation problems, subject to the constraint that in the single phase limit, the pressure equation must be an M -matrix. As mentioned above,

this ensures that the pressure solution retains physically reasonable behaviour. An added bonus is that, when viewed appropriately, the discrete equations have the same form as the usual finite difference control volume formulation. Provided an existing simulation code has a facility for arbitrary cell connectivity [16], it is a simple matter to convert a finite difference code to a control volume-finite element formulation. This has practical significance, since many person-years has gone into the development of existing simulators, which are often 50-100,000 lines of code.

2. Control Volume-Finite Element Method

We will illustrate the basic idea of the method by first examining the discretization of a simple prototype equation:

$$\frac{\partial \rho}{\partial t} = \nabla \cdot (K_r \nabla P) \quad (1)$$

where:

$$\begin{aligned} \rho &= \text{density} \\ K_r &= \text{relative permeability (a function} \\ &\quad \text{of the independent variables)} \\ P &= \text{pressure} \end{aligned}$$

This equation has many of the characteristics of the multi-phase flow conservation laws. Consider the triangle shown in Figure 1. From each side of the triangle, construct a line from the midpoint of the side to a point α in the interior of the triangle. This divides the triangle into “boxes” surrounding each node [17,19,20]. The basic idea of the control volume method is to discretize equation (1) in integrated form:

$$A_i \frac{(\rho_i^{N+1} - \rho_i^N)}{\Delta t} = \int_{S_i} K_r \nabla P \cdot \hat{n} \, ds \quad (2)$$

where A_i is the area of the box surrounding node i . The integral in equation (2) is over the edges e_k (see Figure 1) surrounding node i , and the normal is outward to box i . Let N_i be the usual linear basis functions defined on triangles, $N_i = a_i x + b_i y + c_i$ such that $N_i = 1$ at node i , $N_i = 0$ at all other nodes. Consequently:

$$\begin{aligned} P &= \sum P_i N_i \\ \nabla P &= \sum P_i \nabla N_i \end{aligned} \quad (3)$$

= constant

The discrete form of the right hand side of equation (2) is given by:

$$\int_{S_i} K_r \nabla P \cdot \hat{n} \, ds = \sum_{j \neq i} K_r \left|_{e_j} e_j \nabla P \cdot \hat{n} \right|_{e_j} \quad (4)$$

An upstream weighting for $K_r \left|_{e_j} \right|$ is easy to define. For example, if equation (4) results from the control volume around node 1, then the flux contribution across edge e_2 , is given by:

$$\text{Flux} = K_r \left|_{e_2} e_2 \nabla P \cdot \hat{n} \right|_{e_2} \quad (5)$$

with:

$$\begin{aligned} K_r \left|_{e_2} \right| &= K_r (\text{node } 3) & \nabla P \cdot \hat{n} > 0 \\ &= K_r (\text{node } 1) & \nabla P \cdot \hat{n} < 0 \end{aligned} \quad (6)$$

In order to see the relationships between this method and the usual Galerkin approximation, we will simplify the equation further. Let $K_r = \text{constant} = 1$. In this case, as noted in [19], the integral in equation (4) is independent of the choice of point α , since $\nabla^2 N_i = 0$, so that (for node 1):

$$\int_{S_1} \nabla P \cdot \hat{n} \, ds = d_2 (P_3 - P_1) + d_3 (P_2 - P_1) \quad (7)$$

$$d_i = \ell_k \ell_j \frac{\cos \theta_i}{4A}$$

$A = \text{area of triangle}$

$$= A_1 + A_2 + A_3$$

As noted in [19], this is exactly the same as the row corresponding to node 1 in the local stiffness matrix derived using the usual Galerkin approach:

$$- \int_A \nabla N_1 \nabla P \, dx \, dy = d_2 (P_3 - P_1) + d_3 (P_2 - P_1) \quad (8)$$

If a lumped mass approach is used for the left hand side of equation (1), then discretization of the mass term would be similar to the left hand side of equation (2). The only difference would be that the area A_i surrounding each node would depend on the location of the point α . (The lumped mass approach would give the same area as the control volume method if α was the barycenter of the triangle). For slightly more general equations Bank and Rose [19] show that the control volume and Galerkin methods

methods generate solutions of comparable accuracy, so that both methods are first order correct. Consequently, regardless of point α , we can see that the control volume approach, at least in the single phase limit, is linearly convergent.

It is interesting to note that both techniques give similar discretizations for the flow terms, with only the areas associated with each node being different. This is similar to cell centered and vertex centered finite difference methods on irregular grids. In the finite difference case, both methods also yield the same order of discretization error [21].

Recall from the introduction that an additional constraint on the discretization is that, in the single phase limit, the pressure equation should reduce to an M -matrix. From equation (5) it is clear that a sufficient condition for this constraint is that all interior angles of the triangle must be less than $\pi/2$, which will ensure that d_i are positive. This puts a constraint on the types of triangulation that can be employed. A similar restriction is required for some free boundary problems, [22] which require a discrete maximum principle in conjunction with a finite element method.

From the point of view of discretization error, we are free to choose any convenient point α in the interior of the triangle. If all interior angles are less than $\pi/2$, we can select α to be the intersection of the perpendicular bisectors of the triangle sides. In this case, the flux across e_2 (equation (7)) becomes:

$$\text{Flux} \Big|_{e_2} = d_2 (P_3 - P_1) \quad (9)$$

Note that this is the only choice for e_2 (the perpendicular bisector) which yields the simple form of equation (9), even though the total flux crossing e_2 and e_3 is always given by equation (8). In general, if α was not selected as the intersection of the perpendicular bisectors, then equation (9) would be a function of all three nodal pressures.

In the case that $K_r \neq \text{constant}$, then equation (5) becomes:

$$\text{Flux} \Big|_{e_2} = K_r \Big|_{e_2} d_2 (P_3 - P_1) \quad (10)$$

with $K_r \Big|_{e_2}$ given by equation (6). Note that this form of the flux guarantees that mass will always move from a node with higher pressure to a node with a lower pressure. In general, if α was selected at a different point, it would be possible to have mass flow from node i to node j , even if the pressure in node j was higher than node i . This type of behaviour is unacceptable from an engineering point of view.

From equation (7) and (8), an alternative expression for d_k is:

$$\begin{aligned} d_k &= - \int_A \nabla N_i \cdot \nabla N_j \, dx \, dy \\ &= -\frac{1}{4A} [(y_{i+1} - y_{i+2}) (y_{j+1} + y_{j+2}) \\ &\quad + (x_{i+2} - x_{i+1}) (x_{j+2} - x_{j+1})] \end{aligned} \quad (11)$$

Some straightforward geometry shows that, provided all interior angles are less than $\pi/2$, and α is the intersection of the perpendicular bisectors then equation (11) becomes:

$$d_k = \frac{e_k}{\ell_k} \quad (12)$$

In the case that equation (1) is:

$$\frac{\partial \rho}{\partial t} = (K_x K_r P_x)_x + (K_y K_r P_y)_y \quad (13)$$

where K_x, K_y are possibly functions of (x, y) , then equation (10) becomes:

$$\text{Flux} \Big|_{e_2} = K_y K_r \Big|_{e_2} d_2 (P_3 - P_1) \quad (14)$$

where:

$$\begin{aligned} d_k &= \int_A \left[\left(\frac{K_x}{K_y} \right) (N_i)_x (N_j)_x + (N_i)_y (N_j)_y \right] dx \, dy \\ &= \frac{-1}{4A} \left[\left(\frac{K_x}{K_y} \right) (y_{i+1} - y_{i+2}) (y_{j+1} - y_{j+2}) \right. \\ &\quad \left. + (x_{i+2} - x_{i+1}) (x_{j+2} - x_{j+1}) \right] \end{aligned} \quad (15)$$

where we have assumed that (K_x/K_y) is constant over the triangle.

The condition that d_k are positive is equivalent to requiring that all angles in the triangle obtained by mapping the physical triangle into the (x', y') plane:

$$\begin{aligned} x' &= \frac{x}{\sqrt{K_x}} \\ y' &= \frac{y}{\sqrt{K_y}} \end{aligned} \quad (16)$$

are less than $\pi/2$. If the mapped triangle satisfies this condition, then the pressure equation will be an M -matrix.

The d_k given by equation (15) can be conveniently calculated by the usual finite element assembly procedure. This will produce a “geometric” global stiffness matrix γ_{ij} such that γ_{ij} , $i \neq j$ contains the sum of the d_k from triangles with a common side. Consequently, γ_{ij} contains the entire geometric information about the coupling between node i and node j .

Each local d_k is associated with nodes $i, j \neq k$. As each local d_k is calculated, the total area associated with nodes i and j (A_i^S, A_j^S) is incremented by:

$$\begin{aligned} & \text{(Incremental areas associated with nodes } i, j \text{)} \\ &= \frac{d_k}{4} \left[(y_j - y_i)^2 + \left(\frac{K_y}{K_x} \right) (x_j - x_i)^2 \right] \end{aligned} \quad (17)$$

This incremental area for node i is shown as the shaded area in Figure 2. A_i^S represents the sum of all the incremental areas for all triangles of which node i is a vertex. Consequently, A_i^S represents the area of the box associated with node i .

The final discretization for equation (1) will be:

$$A_i^S \frac{(\rho_i^{N+1} - \rho_i^N)}{\Delta t} = \sum_{j \in \eta_i} K_{y \ j+\frac{1}{2}} K_{r \ j+\frac{1}{2}} (P_j - P_i) \gamma_{ij} \quad (18)$$

where η_i is the set of neighbours of node i , and γ_{ij} is the $(i \ j)$ 'th entry in the global geometric stiffness matrix, and:

$$\begin{aligned} K_{r \ j+\frac{1}{2}} &= K_{ri} \quad \text{if } P_i > P_j \\ &= K_{rj} \quad \text{if } P_j > P_i \end{aligned} \quad (19)$$

Harmonic averaging can be used for $K_{y \ j+\frac{1}{2}}$ [10].

Note that this geometric stiffness matrix need only be calculated once, and the values for γ_{ij} and areas A_i^S stored. Then, equation (18) can be viewed as a discretization of equation (1). Since we are interested in highly non-linear time dependent problems, we would like to avoid the expensive finite element assembly procedure, which would have to be carried out for every Newton iteration. Instead, the Jacobian can be directly constructed from equation (18). Of course, equation (18) has the same form as the usual finite difference discretization of equation (1). The areas and connections

associated with each node have simply been re-defined. However, we have gained considerable flexibility in type of mesh which can be used. Since equation (18) has the same conservative form as difference methods, it is possible to use a very efficient method for constructing the Jacobian [8]. A slightly more general condition can be obtained for generating a triangulation which will produce an M -matrix for the pressure equation. The area of the triangle in Figure 1 is given by:

$$A = \frac{\ell_k \ell_j \sin \theta_i}{2}$$

Restricting attention to the case where $K_x = K_y = \text{constant}$, then equation (7) becomes:

$$d_i = \frac{\cot \theta_i}{2}$$

In general, for interior nodes, the γ_{ij} will contain contributions from two triangles with the common side formed by the edge connecting node i to node j . Consequently:

$$\gamma_{ij} = \frac{\cot \theta_1}{2} + \frac{\cot \theta_2}{2}$$

so that a necessary and sufficient condition for γ_{ij} to be positive is that the sum of the two angles opposite the edge connecting node i to node j must be less than π . A triangulation which satisfies this condition is known as a Delauney triangulation.

Although Delauney triangulations are a generalization of triangulations having all interior angles less than $\pi/2$, for simplicity we will restrict attention in the following examples to local mesh-global mesh couplings with all acute angles.

3. Thermal Reservoir Simulation Equations

The basic equations for modelling steam injection in a dead oil reservoir consist of conservation equations for oil, water (liquid and steam), and heat. Phase velocities are given by Darcy's law for multi-phase systems [10]. The gas phase is taken to be entirely steam, and instantaneous thermal equilibrium is assumed between phases. With the above assumptions, the equations are:

Conservation of oil:

$$\frac{\partial}{\partial t} (\phi S_o M_o) = \nabla \cdot \left\{ M_o \frac{K K_{ro}}{\mu_o} \nabla \psi_o \right\} + q_o \quad (20)$$

Conservation of water:

$$\begin{aligned} & \frac{\partial}{\partial t} (\phi [S_w M_w + S_g M_g]) \\ &= \nabla \cdot \left\{ M_w \frac{K K_{rw}}{\mu_w} \nabla \psi_w \right\} + \nabla \cdot \left\{ M_g \frac{K K_{rg}}{\mu_g} \nabla \psi_g \right\} \\ & \quad + q_w + q_o \end{aligned} \tag{21}$$

Conservation of heat:

$$\begin{aligned} & \frac{\partial}{\partial t} (\phi [S_o M_o U_o + S_w M_w U_w + S_g M_g U_g] + [1 - \phi] U_r M_r) \\ &= \nabla \cdot \left\{ h_o M_o \frac{K K_{ro}}{\mu_o} \nabla \psi_o \right\} + h_o q_o \\ & \quad + \nabla \cdot \left\{ h_w M_w \frac{K K_{rw}}{\mu_w} \nabla \psi_w \right\} + h_w q_w \\ & \quad + \nabla \cdot \left\{ h_g M_g \frac{K K_{rg}}{\mu_g} \nabla \psi_g \right\} + h_g q_g \\ & \quad + \nabla \cdot \lambda_H \nabla T + q_{loss} \end{aligned} \tag{22}$$

where :

- S_ℓ = saturation of phase ℓ
- P_ℓ = pressure of phase ℓ
- T = temperature
- $K_{r\ell}$ = relative permeability of phase ℓ
- μ_ℓ = viscosity of phase ℓ
- K = absolute permeability
- M_ℓ = molar density of phase ℓ
- U_ℓ = internal energy of phase ℓ
- (R = rock)
- h_ℓ = enthalpy of phase ℓ
- q_ℓ = source/sink term for phase ℓ
- q_{loss} = heat loss to surrounding rock strata
- ϕ = porosity
- λ_H = heat conductivity

The phase potentials are given by:

$$\nabla \psi_\ell = \nabla P_\ell - \rho_\ell g \nabla D \quad (23)$$

where:

$$\begin{aligned} \rho_\ell &= \text{mass density of phase } \ell \\ g &= \text{gravitational acceleration} \\ D &= \text{depth} \end{aligned}$$

In addition to above equations, there are the constraints:

$$\begin{aligned} S_o + S_w + S_g &= 1 \\ P_g - P_o &= P_{cg} (S_o + S_w) \\ P_o - P_w &= P_{cw} (S_w) \end{aligned} \quad (24)$$

where P_{cg}, P_{cw} are the capillary pressures. There is also the thermodynamic constraint:

$$\begin{aligned} S_g &= 0 & \text{if } P_{vw}(T) < P_g \\ P_{vw}(T) &= P_g & \text{if } S_g > 0 \end{aligned} \quad (25)$$

where P_{vw} is the water vapour pressure (see the Appendix). Equation (25) governs the appearance/disappearance of the gas (steam) phase. This equation is usually solved as a separate equation along with equations (21-23), to give four equations in the four unknowns (P_o, S_o, S_w, T) [8,11,23]. The properties in equations (21-23), (25), such as viscosities, enthalpies, vapour pressures, etc., are non-linear function, of the independent variables, which are described in the Appendix.

4. Discretization

We will demonstrate the discretization method of the previous section for the oil conservation equation. It is convenient to consider a three dimensional system with thickness Δz , so that the volume associated with each node is:

$$V_i = \Delta z A_i^S \quad (26)$$

with A_i^S defined in equation (18).

Consequently, equation (20) is discretized in the following way:

$$\begin{aligned}
& \frac{V_i}{\Delta t} [(\phi S_o M_o)^{N+1} - (\phi S_o M_o)^N] \\
& = q_{oi}^{N+1} + \sum_{j \in \eta_i} \gamma_{ij} \Delta z \left(\frac{M_o K_{ro}}{\mu_o} \right)_{jup}^L K_{j+\frac{1}{2}} \\
& \quad \{ (P_{oj}^{N+1} - P_{oi}^{N+1}) - \rho_o^L K_{j+\frac{1}{2}} g (D_j - D_i) \}
\end{aligned}$$

where γ_{ij} is the entry in the global geometric stiffness matrix (equation (18)), N is the timestep number, and $K_{j+\frac{1}{2}}$ is computed using the harmonic mean [10].

The term:

$$\left(\frac{M_o K_{ro}}{\mu_o} \right)_{jup}^L \quad (28)$$

is evaluated at the upstream point as determined by the sign of:

$$(P_{oj}^{N+1} - P_{oi}^{N+1}) - \rho_o^L K_{j+\frac{1}{2}} g (D_j - D_i) \quad (29)$$

An adaptive implicit method is used for timestepping [24-27], so that superscript L is either $L = N$ or $L = N+1$, depending on the state of node j_{up} .

The other equations (22-23) are discretized in a similar fashion. Full Newton iteration is used to solve the resulting set of non-linear algebraic equations. A detailed description of the adaptive implicit method, Jacobian construction, and matrix solve is given in [25]. Since the form of equation (27) is similar to the form of the usual finite difference equations, the methods of Reference [25] can be used with only the slight generalization to nodes with an arbitrary number of neighbours.

5. Cyclic Steam Cross Section

In order to compare a locally refined grid (discretized with the control volume-finite element technique) and the usual finite difference grid, we will adopt the following procedure. Given a typical finite difference grid, a locally refined grid will be constructed by coarsening certain regions of the finite difference grid. The objective is to show that essentially the same predictions can be obtained with a control volume - finite element grid compared with a typical finite difference grid, but at much reduced cost. We will not attempt to demonstrate convergence to a solution, because of the computational cost involved. In any case, this is rarely done in practice. Since comparatively coarse grids are being used, we can expect some differences in the results obtained using different discretizations.

Figure 3 shows a typical finite difference grid for a cross sectional cyclic steam injection problem with a horizontal well. The various physical properties are given in the Appendix. The oil viscosity is initially very high, and the idea of cyclic injection is to inject steam for a limited period of time, followed by a soak period, and then to produce from the same well. Oil is produced from the heated zone near the well, since oil viscosity decreases very quickly with increasing temperature.

For this problem, 70% quality steam was injected at 327 °C, at a cold water equivalent rate of $5 m^3/\text{day}$ per meter of horizontal well length. One complete cycle of a 10 day injection, 10 day soak, followed by 10 days of production was simulated. The well was produced at a bottom hole pressure of 100 *kpa*, subject to a maximum fluid rate of $10 m^3/\text{day}$ per meter of well length.

This problem was run on both the conventional 13×8 difference grid shown in Figure 3 (the global grid), and the locally refined grid obtained using a control volume-finite element grid shown in Figure 4. The dotted lines in Figure 4 represent the triangulation used to obtain the global geometric stiffness matrix γ_{ij} . However, the dotted lines represent connections which are identically zero. These connections are not included in the neighbour lists η_i . The same code was used in both cases, with the neighbour lists η_i , nodal volumes, and connection factors reflecting the particular choice of grid.

Table 1 shows the cumulative oil production per meter of well length after the ten day production period. Note that the difference in comulatives between the global and local grids is less than 2%.

The actual oil rates for both grids are shown in Figure 5. Rapid changes in oil rate occur in the first day days after production due to the sudden drop in wellbore pressure, which causes flashing of steam. Also, the well operating constraint switches from pressure, to maximum fluid rate, and finally back to pressure during the first few days. However, the oil rates for both grids are in reasonable agreement.

Table 2 gives the CPU times for both grids using a fully implicit and adaptive implicit timestepping method [24-27]. In both cases, an approximate 40% reduction in CPU time was achieved, while obtaining virtually the same predictions for oil production. Note that use of the adaptive implicit method combined with local mesh refinement is almost four times faster than a fully implicit method on a conventional grid. A fully implicit, finite difference method is the standard approach for solving these problems [9].

6. Steam Injection into a Fracture

Figure 6 shows a conventional areal finite difference grid, with a fracture in the lower right corner. The reservoir is taken to be 10 m thick. Fractures are often produced by the high pressures resulting from steam injection [28]. The fracture is modelled by using very thin cells (approximately .01 m in width) with very large permeabilities (10^6 md). Figure 6 shows a 14×13 grid (note that the grid line extension of the fracture is too small to be seen).

The same problem was run on the control volume-finite element grid shown in Figure 7 (the local grid).

Steam (327°C , 70% quality) was injected into the fracture at a cold water equivalent rate of $50\text{ m}^3/\text{day}$ for ten days. A ten day soak period followed, and then the fracture was produced for ten days. The injection/production well was placed in the lower right corner of the fracture. The well was produced at a bottom hole pressure of 100 kpa, subject to a maximum fluid rate of $50\text{ m}^3/\text{day}$. Other relevant physical data are given in the Appendix.

Figure 8 shows the oil rates predicted for both the local and global grids. After two days of production, both methods are in good agreement. However, during the first few days of production, the oil rate oscillates rapidly. Detailed examination of the output revealed that the sudden drop in wellbore pressure at the onset of the production cycle caused the appearance of superheated steam in several cells adjacent to the well. During this period the well constraint also switched from pressure, to maximum fluid rate, and back to pressure.

Very small differences in nodal pressures and temperature between the two runs were enough to trigger slightly different numbers of superheated nodes, and this also affected the timing of the constraint switches. This can be seen from the shift in the peak production rates of the two curves in Figure 8. In short, this problem should be viewed as an extremely pathological test of the ability of the local grid to reproduce the results of the global grid.

Table 3 shows the cumulative oil productions for both grids. In this case, the cumulatives differ by approximately 10%. This is all due to the different oil rates predicted during the extremely sensitive period which follows the beginning of the production cycle. However, the difference between the two runs, even in this pathological case, is probably insignificant in practical situations with uncertain geological data.

Table 4 gives the execution times for both the grids (local and global) shown in Figures 6 and 7. Note that the local grid solution requires approximately 50% less CPU time than the global grid. The adaptive implicit technique was used for both runs.

7. Conclusions

A control volume-finite element technique has been developed for reservoir simulation problems, based on triangular mesh elements. The pressure is discretized in a finite element manner, while a control volume approach allows upstream weighting of the phase mobilities. The cell volumes and edges are consistent with the linear finite element discretization of the pressure. Provided certain restrictions are placed on the geometry of the triangles, this technique will produce an M -matrix for the pressure in the single phase limit. This means that no non-physical local maxima and minima can appear in the pressure solution. In the multi-phase case, we have also ensured that mass can only flow from nodes with higher phase potential to nodes at lower phase potential. This also prevents non-physical behaviour.

In the single phase limit, this technique can be viewed as a special type of finite element method [19], and so the pressure is at least first order correct in terms of discretization error. The usual finite element assembly procedure can be used to obtain all the geometric factors required for the final discrete equations. These final equations have the same form as the usual control volume type equations, except that the cell volumes, interfacial areas, and neighbour lists have been redefined. Consequently, it is a simple matter to implement this technique in any existing simulator with an arbitrary cell connectivity facility. This also means that standard iterative techniques can be used to solve the Jacobian matrix [29], since the Jacobian also has similar properties compared to the usual control volume discretization.

The control volume-finite element method has been demonstrated as a means of coupling local fine meshes with global coarse meshes. On the same example thermal cyclic steam simulations, the local mesh gives comparable predictions to the global fine mesh at 40-50% less computing cost. It is interesting to note that an adaptive implicit - local mesh solution is almost four times faster than the standard fully implicit global mesh approach.

Although this technique has been demonstrated in conjunction with local mesh refinement, it can be used as a general method for discretization. The use of a triangulation gives great flexibility in construction of a mesh. Consequently, the control volume - finite element method has great potential for widespread use in reservoir

simulation.

8. Acknowledgements

This work was supported by the National Sciences and Engineering Research Council of Canada and by the Information Technology Research Center funded by the Province of Ontario.

9. Nomenclature

A	area of triangle
A_i	area of triangle associated with node i
A_i^S	sum of all associated areas for all triangles with i as vertex
d_i	finite element pressure coupling term
D	depth
e_j	edge of box in triangle (see Figure 1)
g	gravitational acceleration
h	enthalpy
K_r	relative permeability
K	absolute permeability
ℓ_k	length of side of triangle (Figure 1)
M	molar density
N_i	linear triangular basis function associated with node i
\hat{n}	unit normal to edge e
P	pressure
P_{cg}	liquid-gas capillary pressure
P_{cw}	oil-water capillary pressure
P_{vw}	water vapour pressure
q	source/sink term
$q\ell_{oss}$	heat loss to surrounding rock strata
S	saturation
T	temperature
U	internal energy
V_i	volume associate with node i
x_i	x -coordinate of node i
y_i	y -coordinate of node i
Δz	mesh spacing in z -direction
α	point in the interior of a triangle

ρ	density
γ_{ij}	entry in global geometric stiffness matrix connecting node i with node j
ϕ	porosity
μ	viscosity
ψ	phase potential
λ_h	heat conductivity
η_i	set of vertices neighbouring node i

Subscripts

o	oil
g	gas
w	water
r	rock
j_{up}	upstream

Superscripts

N, L	time level
--------	------------

References

- [1] Z.E. Heinemann, G. Gerken, G. von Hantelmann, "Using Local Grid Refinement in a Multiple Application Reservoir Simulator," SPE 12255 presented at the 7th SPE Symposium on Reservoir Simulation, San Francisco, 1983.
- [2] P. Quandalle, P. Besset, "The Use of Flexible Gridding for Improved Reservoir Modelling," SPE 12239 presented at the 7th SPE Symposium on Reservoir Simulation, San Francisco, 1983.
- [3] P.A. Forsyth, P.H. Sammon, "Local Mesh Refinement and Modelling of Faults and Pinchouts," SPE J. Form. Eval., 1 (1986) 275-285.
- [4] P. Quandalle, P. Besset, "Reduction of Grid Effects Due to Local Sub-Gridding in Simulations Using a Composite Grid," SPE 13527 presented at the 8th SPE Symposium on Reservoir Simulation, Dallas, 1985.
- [5] D.K. Han, D.L. Han, C. Zan, L. Peng, "A More Flexible Approach of Dynamic Local Grid Refinement for Reservoir Modelling," SPE 16014 presented at the 9th SPE Symposium on Reservoir Simulation, San Antonio, 1987.
- [6] O. Pederosa, K. Aziz, "Use of a Hybrid Grid in Reservoir Simulation," SPE 13507 presented at the 8th SPE Symposium on Reservoir Simulation, Dallas, 1985.
- [7] K.H. Coats, "In-Situ Combustion Model," Soc. Pet. Eng. J. 20 (1980) 533-554.
- [8] B. Rubin and W.L. Buchanan, "A General Purpose Thermal Model," paper SPE 11713 presented at the 1983 California Regional Meeting, Ventura, California.
- [9] K. Aziz, A.B. Ramesh, and P.T. Woo, "Fourth SPE Comparative Solution Project - A Comparison of Steam Injection Simulators," paper SPE 13510, presented at the 8th SPE Symposium on Reservoir Simulation, Dallas, 1985.
- [10] K. Aziz and A. Settari, "Petroleum Reservoir Simulation," Applied Science, London.
- [11] P.A. Forsyth, B. Rubin, P.K.W. Vinsome, "The Elimination of the Constraint Equation and Modelling of Problems with a Non-condensable Gas in Steam Simulation," J. Can. Pet. Tech. #4 (1981) 63-68.

- [12] P.H. Sammon, "An Analysis of Upstream Differencing," submitted to Soc. Pet. Eng. J. Res. Eng. (1986).
- [13] M. Osborne and J. Sykes, "Numerical Modelling of Immiscible Organic Transport at the Hyde Park Landfill," Water Res. Res. 22 (1986) 25-33.
- [14] P.A. Forsyth, P.H. Sammon, "Local Mesh Refinement and Modelling of Faults and Pinchouts," SPE J. Form. Eval. 1 (1986) 275-285.
- [15] R. Varga, "Matrix Iterative Analysis," Prentice-Hall, 1962.
- [16] P. Quandalle and J.C. Sabathier, "Typical Features of a New Multipurpose Reservoir Simulator," Proc. 9th SPE Symposium on Reservoir Simulation, San Antonio, 1987.
- [17] C. Prakash, "Examination of the Upwind Formulation in the Control Volume Finite-Element Method for Fluid Flow and Heat Transfer," Num. Heat Transfer 11 (1987) 401-416.
- [18] G. Schneider, M.J. Raw, "A Skewed, Positive Influence Coefficient Upwind-ing Procedure for Control Volume Based Finite Element Convection Diffu-sion Computation," Num. Heat Trans. 9 (1986) 1-26.
- [19] R. Bank, D. Rose, "Some Error Estimates for the Box Method," SIAM J. Num. Anal. 24 (1987) 777-787.
- [20] S. Polak, C. Den Heijer, H. Schilders, P. Markowich, "Semiconductor Device Modelling From a Numerical Point of View," 24 (1987) 763-838.
- [21] P.A. Forsyth, P.H. Sammon, "Quadratic Convergence of Cell Centered Grids," Appl. Num. Math. (to appear).
- [22] L. Marini, P. Pietra, "Fixed Point Algorithms for Stationary Flow in Porous Media," Comp. Meth. Appl. Mech. Eng. 56 (1986) 17-45.
- [23] T.B. Tan, "Implementation of an Improved Adaptive Implicit Method in a Thermal Compositional Simulator," paper SPE 16028 presented at the 9th SPE Symposium on Reservoir Simulation, San Antonio, 1987.
- [24] G.W. Thomas, D.H. Thurnau, "Reservoir Simulation Using An Adaptive Implicit Method," Soc. Pet. Eng. J. 23 (1983) 750-768.
- [25] P.A. Forsyth, P.H. Sammon, "Practical Considerations for Adaptive Implicit Methods in Reservoir Simulation," J.Comp. Phys. 62 (1986) 265-281.

- [26] P. Quandalle, J.C. Sabathier, “Typical Features of a New Multipurpose Reservoir Simulator,” paper SPE 16007 presented at the 9th SPE Symposium on Reservoir Simulation, San Antonio, 1987.
- [27] G.A. Behie, P.A. Forsyth, P.H. Sammon, “Adaptive Implicit Methods Applied to Thermal Simulation,” Soc. Pet. Eng. J. Res. Eng. 2 (1987) 596-598.
- [28] S.K. Wong, “Analysis and Implications of In-situ Stress Changes During Steam Stimulation of Cold Lake Oil Sands,” Soc. Pet. Eng. J. Res. Eng. 3 (1988) 55-61.
- [29] A. Behie, P.A. Forsyth, “Incomplete Factorization Methods for Fully Implicit Simulation of Enhanced Oil Recovery,” SIAM J. Sci. Stat. Comp. 5 (1984) 543-561.

Appendix

This Appendix gives the physical data for the cyclic steam examples. The relative permeabilities are given in Table 5. Stone’s model [10] is used for the three phase relative permeability. Other relevant data are:

Absolute permeability ($K_x = K_y$)	100 <i>md</i>
Absolute permeability in the fracture	$K_x = 100 \text{ } md$ $K_y = 10^6 \text{ } md$
Porosity	.3
Rock compressibility	$5 \times 10^{-6} \text{ } (kpa)^{-1}$

Molar densities

$$M_w = M_{wr} [1 + \alpha_w (P - P_r) - \beta_w (T - T_r)] \text{ } mol/m^3$$

$$M_{wr} = 5.55 \times 10^4 \text{ } mol/m^3$$

$$\alpha_w = 4.3 \times 10^{-6} \text{ } (kpa)^{-1}$$

$$\beta_w = 2.1 \times 10^{-4} \text{ } (^{\circ} K)^{-1}$$

$$T_r = 273 \text{ } ^{\circ} K$$

$$P_r = 100 \text{ } kpa$$

$$M_o = M_{or} [1 + \alpha_o (P - P_r) - \beta_o (T - T_r)] \text{ } mol/m^3$$

$$M_{or} = 4.1 \times 10^3 \text{ } mol/m^3$$

$$\alpha_o = 3 \times 10^{-6} \text{ } (kpa)^{-1}$$

$$\beta_o = 2 \times 10^{-4} \text{ } k \text{ } ^{\circ} K)^{-1}$$

$$M_g = P/R T \text{ } mol/m^3$$

Molar mass

$$\text{Water} \quad 18 \times 10^{-3} \text{ kg/mole}$$

$$\text{Oil} \quad .170 \text{ kg/mole}$$

Enthalpies

$$h_o = C_o (T - T_r)$$

$$C_o = 242 \text{ J/(mole} - ^\circ K)$$

$$h_w = C_w (T - T_r)$$

$$C_w = 75.4 \text{ J/(mole} - ^\circ K)$$

$$h_g = C_w (T_s - T_r) + h_{lat} + C_g (T - T_s)$$

$$C_g = 30.5 \text{ J/(mole} - ^\circ K)$$

$$T_s = 243 + [P_g / (.877 \times 10^{-8})^{(1/4.76)}] ^\circ K$$

$$P_g = \text{pressure in kpa}$$

$$h_{lat} = 4.814 \times 10^3 (T_{cr} - T_s)^{.38} \text{ J/mole}$$

$$T_{cr} = 647.3 ^\circ K$$

Vapour pressure of water

$$P_{vw} = .877 \times 10^{-8} (T - 243.0)^{4.76} \text{ kpa}$$

$$T = \text{temperature in } ^\circ K$$

Viscosities

Water

$$= \frac{10^{-9}}{[12.1 + 2.88 (T - 273) + 7.78 \times 10^{-4} (T - 273)^2]} \text{ kpa} - \text{day}$$

Steam

$$= 10^{-13} [1.574 + .44 (T - 273)] \text{ kpa} - \text{day}$$

Oil

(See Table 6)

Heat Capacity of rock

$$U_r \ M_r = 2.35 \times 10^6 \ J/(M^3 - ^\circ K)$$

Heat loss

No heat loss permitted

Capillary pressure

Both gas and water capillary pressure are set equal to zero.

Initial data

Temperature	367 °K
Oil saturation	.8
Water saturation	.2
Pressure	500 <i>kpa</i>

Table 1

Cumulative oil production at 30 days for the global and locally refined grid solutions of the cyclic steam cross section problem.

Cumulative Oil Production (m^3/m of wellbore)	
Global Grid (Figure 3)	3.10
Locally Refined (Figure 4)	3.04

Table 2

Comparison of the execution times for the global and locally refined grid solutions of the cyclic steam cross section problem.

Method	Execution Time (VAX 11/785 seconds)	
	Global Grid (Figure 3)	Locally Refined (Figure 4)
Fully Implicit	995	627
Adaptive Implicit	449	272

Table 3

Cumulative oil production at 30 days for the global and locally refined grid solutions of the fractured cyclic steam example.

Cumulative Oil Production (m^3)

Global Grid (Figure 6)	29.7
Locally Refined (Figure 7)	33.1

Table 4

Comparison of execution times for the global and locally refined grid solutions of the fractured cyclic steam example.

Execution Time (Vax 11/785 seconds)

Global Grid (Figure 6)	1259
Locally Refined (Figure 7)	656

Table 5

Relative permeability curves used for the cyclic steam examples.

S_w	K_{rw}	K_{ro}
.2	0.0	.88
.3	.04	.55
.4	.10	.43
.5	.18	.31
.6	.30	.20
.7	.44	.12
.8	.60	.05
.9	.80	0.0
1.0	1.0	0.0

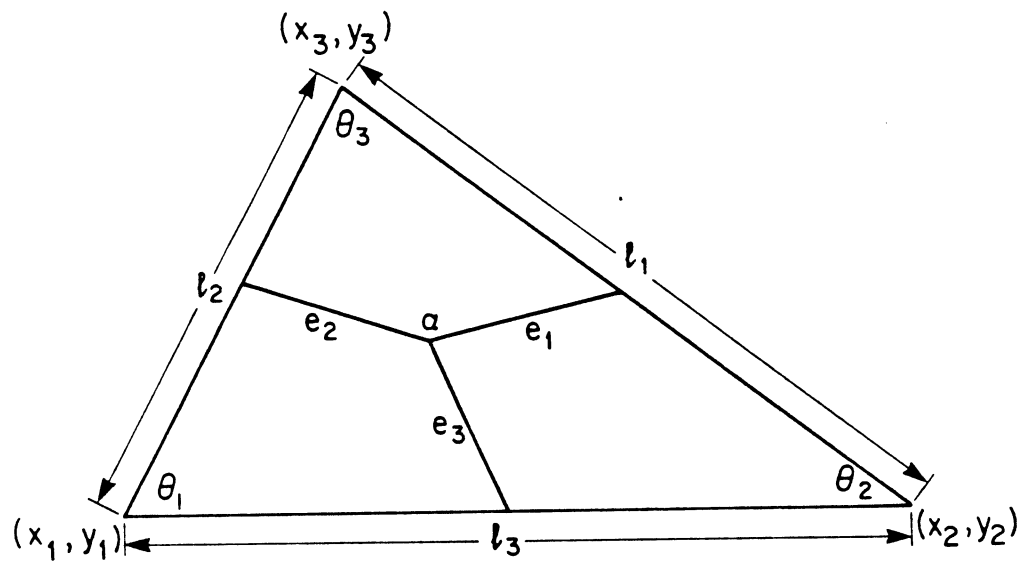
$S_o + S_w$	K_{rg}	K_{ro}
.2	1.0	0.0
.3	.75	0.0
.5	.35	.005
.6	.21	.12
.8	.04	.34
.95	0.0	.58
1.0	0.0	.68

Table 6

Oil Viscosity for the cyclic steam examples.

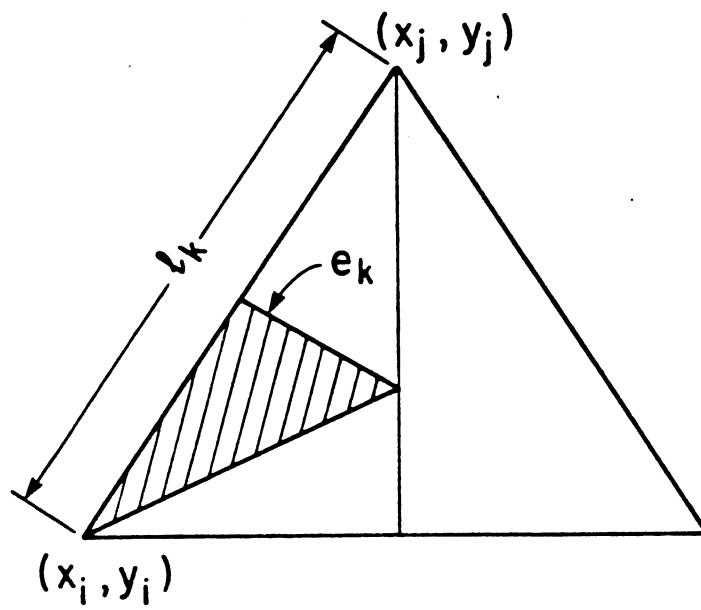
$T(^{\circ}K)$ $\mu_o(cp)$	
310	1380
338	187
366	47
394	17.4
421	8.5
449	5.2
533	2.5
700	1.0

Figure 1



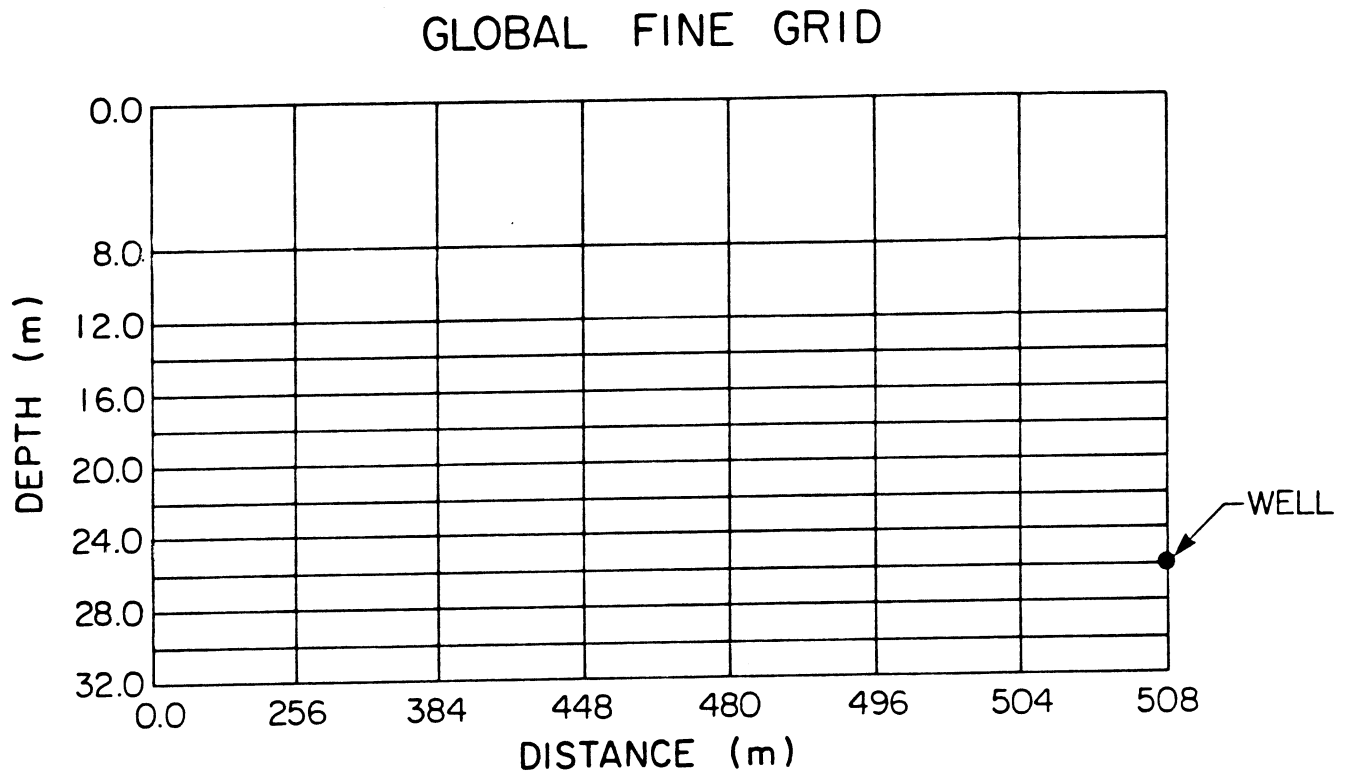
Basic triangular mesh element.

Figure 2



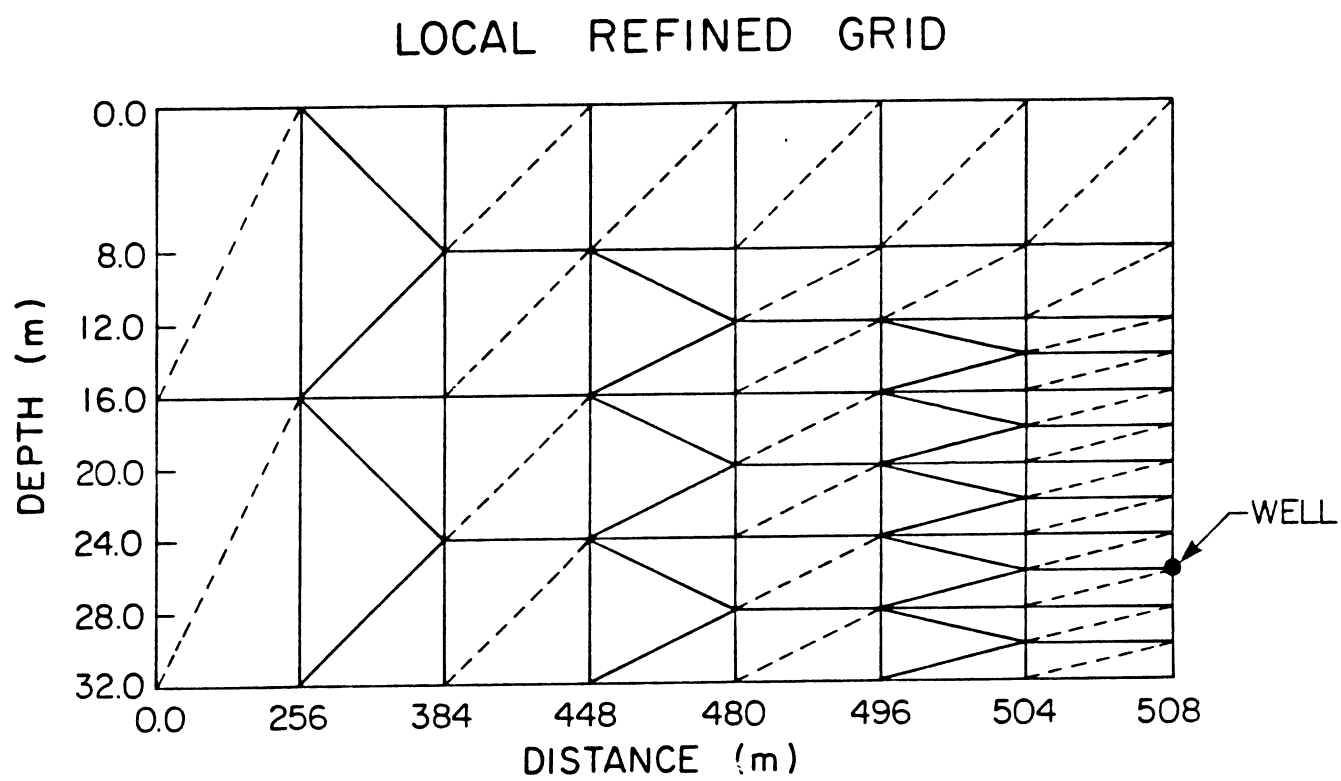
Incremental area associated with node i from edge e_k .

Figure 3



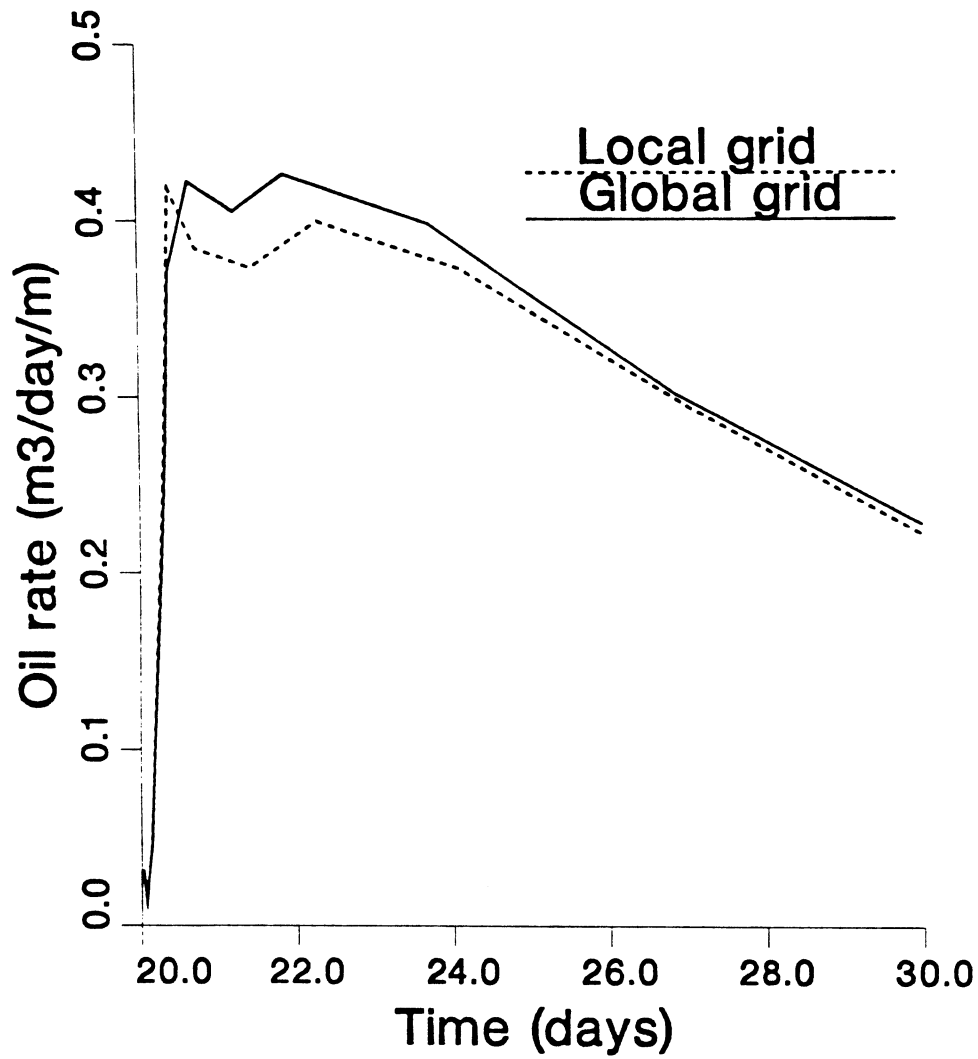
Typical global grid for cross-sectional cyclic steam problem.

Figure 4



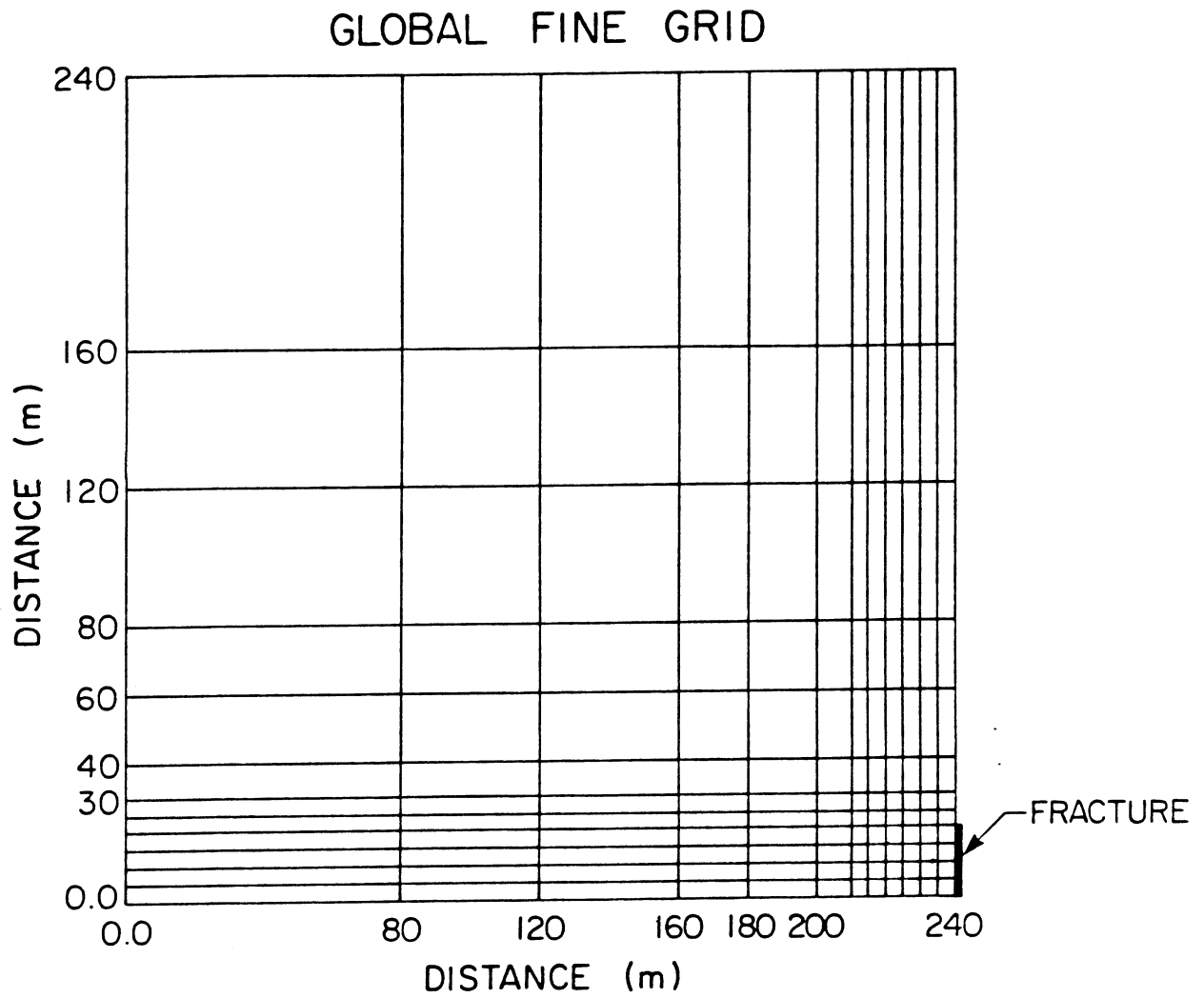
Locally refined version of the grid shown in Figure 3.

Figure 5



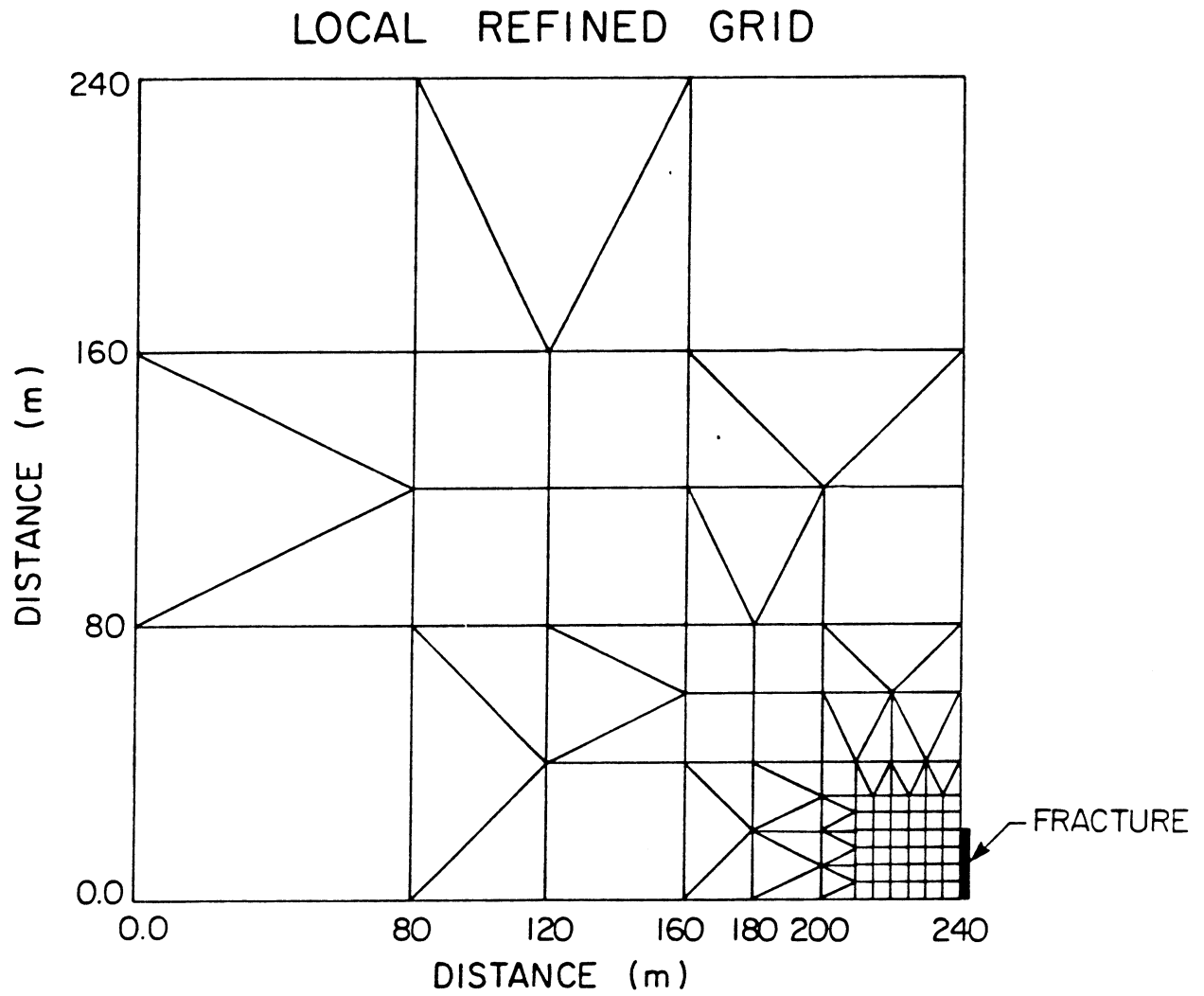
Comparison of oil rates for the locally refined and conventional global grid for the cyclic steam cross section.

Figure 6



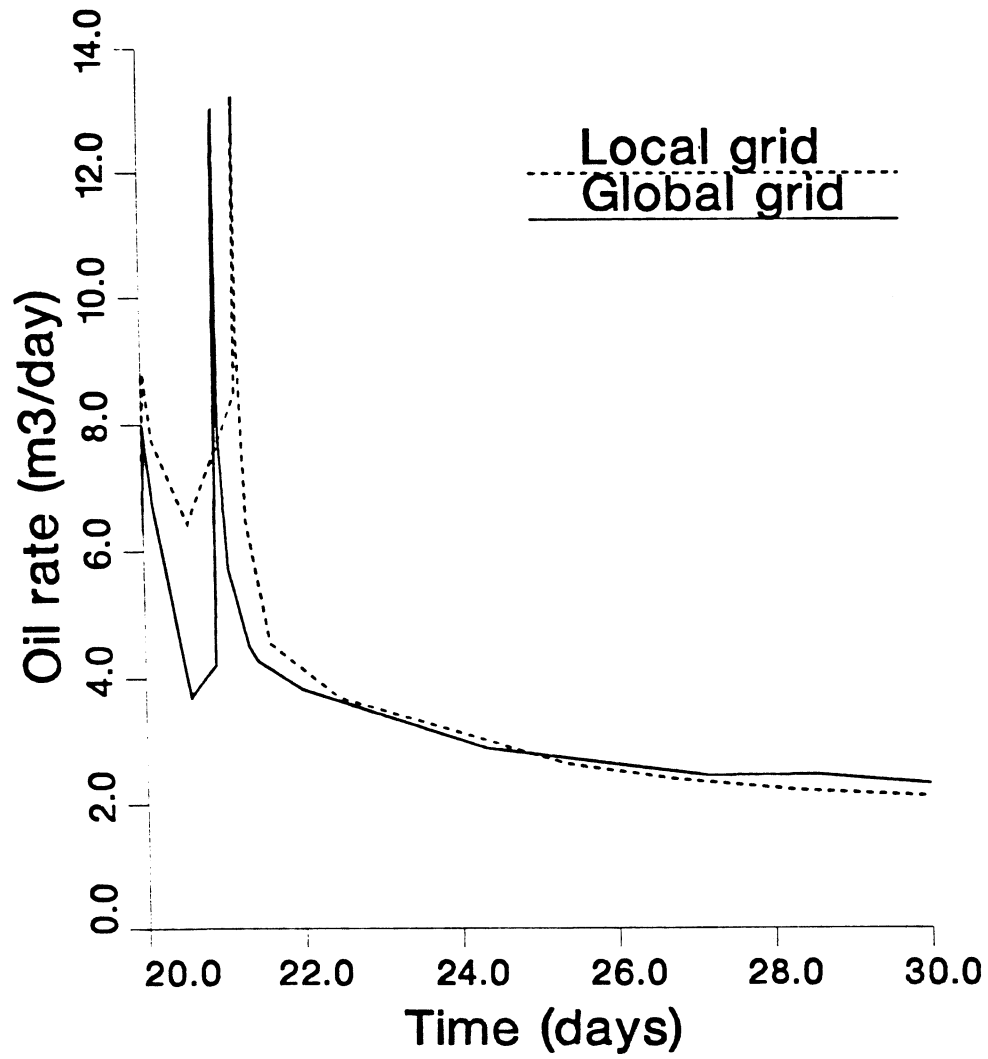
Typical global grid for simulation of an areal fracture problem.

Figure 7



Locally refined version of the grid shown in Figure 6.

Figure 8



Comparison of oil rates for the locally refined grid and conventional global grid for the fracture problem.